International Journal of Heat and Mass Transfer 195 (2022) 123129

Contents lists available at ScienceDirect

International Journal of Heat and Mass Transfer

journal homepage: www.elsevier.com/locate/hmt

Design and multi-objective optimization of a new annular constructal bifurcation Stirling regenerator using response surface methodology

Minjie Yu, Chunyu Shi, Zhichun Liu, Wei Liu*

School of Energy and Power Engineering, Huazhong University of Science and Technology, Wuhan 430074, China

ARTICLE INFO

Article history:
Received 24 May 2021
Revised 31 May 2022
Accepted 8 June 2022

Keywords:
Stirling engine
Constructal bifurcation regenerator
Response surface methodology
Multi-objective optimization
Irreversible loss

ABSTRACT

The irreversible losses such as the flow loss and axial heat conduction loss in traditional porous regenerators have limited the specific power and thermal efficiency of Stirling engines to a great degree. Thereby, the objective of this paper is to design and optimize a novel annular constructal bifurcation regenerator for diminishing the flow and axial heat conduction losses in the regenerator based on constructal concept and response surface methodology. First, the bifurcation type structure units with an inclined angle to the flow direction and the layered approach were applied to construct the regenerator matrix. Thereafter, the numerical simulations were employed to investigate the gas flow and heat transfer characteristics of the constructal bifurcation regenerator. Based on the numerical data, the quadratic polynomial regression models between the geometric parameters and the regenerator performance were established using response surface methodology, and the specific effects of the geometric dimensions were analyzed via 2-D and 3-D response surface plots. Subsequently, a multi-objective optimization was conducted to minimize the flow resistance and maximize the heat transfer rate by genetic algorithm. A most eclectic solution with the global friction factor $f = 3.478$ and the number of heat transfer units $NTU = 1.135$ was selected from the optimal Pareto front. Finally, the overall performance of the constructal bifurcation regenerator was compared with that of the porous regenerator and the parallel geometry regenerator. The results indicate that a low flow resistance, low axial heat conduction, and high thermal performance are obtained by the constructal bifurcation regenerator. Therefore, it is reasonable to conclude that the annular constructal bifurcation regenerator achieves a high comprehensive performance, with the potential to improve the performance of Stirling engines. The findings of this paper may provide some new ideas and guidelines for the design and optimization of the regenerator structures.

1. Introduction

The concept of sustainable development has been embedded deeply in our minds since it was first put forward by the UN in 1987 [1]. The use of renewable and clean energy plays an increasingly important role in achieving sustainable development goals. Stirling engines have become one of the most promising renewable energy utilization technologies due to their most remarkable advantages of the flexibility in selecting the energy resource, along with other advantages such as high thermal efficiency, low noise, and maintenance requirements [2]. As one of the crucial components of Stirling engines, the regenerator can improve the overall performance of the engines significantly. The regenerator is made up of a void filled with a solid matrix. When the hot gas flows into the regenerator from the hot end, the solid matrix absorbs heat from the gas. Conversely, as the cold gas flows back through the regenerator from the cold end, the solid matrix releases the heat stored in the previous half-cycle back into the gas. Resulted from the periodic heat absorption and release, a large temperature difference is generated between the hot and cold ends of the regenerator, thus improving the thermal efficiency of the Stirling engine [3]. According to the research of Tavakolpour et al. [4], the thermal efficiency for a Stirling engine with an ideal regenerator can reach six times the one of a Stirling engine without the regenerator.

Currently, the most widely used regenerator matrix type in Stirling engines is the conventional porous media such as the woven screen and random fiber. Therefore, numerous studies have been conducted to understand the hydraulic and thermal characteristics of these regenerators and to explore their effects on the compre-

Abbreviations: ANOVA, analysis of variance; CBR, constructal bifurcation regenerator; CCD, central composite design; CFD, computational fluid dynamics; DF, degrees of freedom; DOE, design of experiments; NSGA-II, fast non-dominated sorting genetic algorithm; RSM, response surface methodology; TOPSIS, technique for order preference by similarity to ideal solution.

* Corresponding author.
E-mail address: w_liu@hust.edu.cn (W. Liu).

https://doi.org/10.1016/j.ijheatmasstransfer.2022.123129
0017-9310/

Nomenclature

A, B, C, D	variable codes in the response surface analysis
a_r	specific surface area of the regenerator matrix, m^{-1}
A_r	surface area of the regenerator matrix, m^2
b	number of center points
$c_{p,f}$	specific heat of the gas, J/(kg·K)
$c_{p,s}$	specific heat of the solid, J/(kg·K)
d_h	hydraulic diameter of the regenerator matrix, mm
D_i	inner diameter of the regenerator, mm
D_o	outer diameter of the regenerator, mm
d_w	wire diameter, mm
e	statistical error
f	global friction factor
f_h	friction factor based on the hydraulic diameter
h	convective heat transfer coefficient, $W/(m^2 \cdot K)$
h_l	total heat transfer coefficient per unit length, $W/(m^3 \cdot K)$
k	turbulent kinetic energy, m/s^2
L	regenerator length, mm
$\dot{m}$	mass flow rate of the gas, kg/s
n	number of the design variables
NTU	number of heat transfer units
Nu_h	Nusselt number based on the hydraulic diameter
p	pressure, Pa
q	heat flux, W/m^2
R^2	coefficient of determination
Re_h	hydraulic Reynolds number
Re_{in}	inlet Reynolds number
s	wire mesh pitch, mm
t	time, s
T_f	temperature of the gas, K
T_s	temperature of the matrix solid, K
u	bulk velocity of the gas, m/s
$\boldsymbol{u}$	velocity vector, m/s
u_{in}	velocity at the inlet of the regenerator, m/s
V	total volume of the regenerator, m^3
V_s	matrix solid volume of the regenerator, m^3
x, y, z	coordinate axis
x_i, x_j	design variables
Y	objective response

Greek symbols

α_0, α_i, α_{ii}, α_{ij}	regression coefficients of the model
β	inclined angle of the wire mesh, °
γ	porosity
ε	turbulent dissipation rate, m^2/s^3
θ	central angle of the wire mesh, °
λ_f	thermal conductivity of the gas, W/(m·K)
λ_s	thermal conductivity of the matrix solid, W/(m·K)
μ	viscosity of the gas, Pa·s
μ_{in}	viscosity of the gas at the inlet of the regenerator, Pa·s
ρ_f	density of the gas, kg/m^3
ρ_{in}	density of the gas at the inlet of the regenerator, kg/m^3
ρ_s	density of the matrix solid, kg/m^3

hensive performance of Stirling engines. Numerical studies were developed to characterize the pressure drop [5] and heat transfer [6] phenomenon of the woven screen regenerator matrix. Other numerical simulations investigated temperature distribution characteristics in the regenerator [7] and compared the performance of Stirling engines for the cases with and without regenerators [8,9] at the engine level. Analytical studies were conducted to discuss the influence of multi-mesh regenerator [10] and temperature oscillation in regenerator matrix [11] on the engine performance. A combined analytical and numerical work developed a new differential model to evaluate the regenerator efficiency of an α-type Stirling engine and validated it with a CFD simulation [12]. Experiments were performed to quantify the flow resistance [13] and thermal performance [14] and to obtain the correlations for friction factor and Nusselt number [15,16] of the porous regenerator in the oscillating flow. Other experimental investigations explored the effects of moving regenerators [17] and the temperature difference between both regenerator sides [18] on the power output of Stirling engines. Combined experimental and numerical studies were carried out to strengthen the understanding of oscillating flow characteristics of the regenerator [19] and to compare the difference between the oscillating and steady flows [20]. These studies show that the conventional porous regenerators offer an excellent heat transfer performance due to the large specific surface area and high convective heat transfer coefficient. Nevertheless, a high flow loss will be inevitably caused by the prevalent flow separation and eddy structures as the gas flows through these regenerators. In addition, the axial heat conduction loss resulted from the large axial temperature gradient and the close contact between the microstructures of the solid matrix in these regenerators cannot be disregarded. These losses will lead to a significant decrease in engine power output and thermal efficiency. Consequently, it is vitally important to design a regenerator with low pressure drop and axial thermal conduction for the performance improvement of Stirling engines.

In the latest years, parallel geometry type regenerators have attracted much attention from researchers. A few new conceptual parallel geometry type regenerators, such as parallel wire regenerators [21], involute-foil regenerators [22,23], layered-plate regenerators [24], micro-channel type stacked porous sheets regenerators [25,26], circular miniature-channels regenerators [27,28], and robust foil regenerators [29], were continually developed and investigated. As opposed to conventional porous regenerators, these types of regenerators show a great superiority in pressure drop characteristics because of their smooth flow passage. However, due to the lack of disturbance in the flow, the thermal performance of these regenerators is evidently reduced. Besides, higher axial heat conduction loss seems to be generated by the parallel geometry type regenerators compared with the porous regenerators. Therefore, another new type of regenerator with different design ideas is required to achieve a low flow resistance, low axial heat conduction, and relatively high thermal performance.

The performance of the regenerator is strongly affected by the angle between the extension direction of the matrix surface and the gas flow direction [17]. Theoretically, if the matrix surface is parallel to the flow direction, the regenerator reaches its minimum value in terms of flow resistance but accompanying by a relatively poor thermal performance. On the contrary, if the matrix surface is perpendicular to the flow direction, the regenerator will have the maximum flow loss and high heat transfer rates. Hence, to obtain a low flow loss and relatively high heat transfer performance, it may be a reasonable attempt to design a regenerator with the matrix surface inclined to the gas flow direction. Meanwhile, for the achievement of a relatively uniform spatial distribution and a large heat transfer surface area of the solid matrix, the well-known constructal concept in structure optimization can be introduced to guide the regenerator matrix design. Since the constructal concept was first proposed by Bejan in 1996 [30], it has been extensively employed in various engineering practices [31–35] in the past few decades, in which the constructal concept provided

a universal guideline for structure design and optimization. However, to date, with the exception of a study previously published by the authors [36], no more attempts have been made to design Stirling regenerators using the constructal concept in the published literature. In the previous work of the authors, a cylindrical constructal bifurcation regenerator with a central connecting rod was first developed based on the constructal concept. The transient flow and thermal characteristics of the regenerator in the oscillating flow were investigated. Compared with other regenerators, the cylindrical constructal bifurcation regenerator has a low flow resistance and moderate heat transfer performance, thus achieving a relatively high overall performance. Nevertheless, the cylindrical overall configuration limits the application of the regenerator almost exclusively for α type Stirling engines. Compared with the α type, β and γ types of Stirling engines have higher power density and thermal efficiency [37], which have drawn more attention. In general, an annular regenerator is used in these types of Stirling engines. Therefore, it is essential to develop an annular regenerator using the constructal concept to fill the gap where no constructal concept-based regenerator is applied to β and γ types of Stirling engines.

In addition, as can be concluded from the previous studies related to the regenerators, geometric parameters have a significant effect on the overall performance of the regenerators, so the optimization of the geometric parameters of the regenerator is of great value for improving the performance of the regenerator. Several studies have been conducted to optimize the different regenerator parameters such as housing aspect ratios [38], porosities [39], wire diameter [40], and the number of sub-regenerators [41]. However, these studies were mostly based on single-factor parametric or thermodynamic analyses, lacking the rigorous simultaneous optimization of multi-factors in the mathematical and statistical sense. One of the extensively used mathematics and statistics based optimization methods is the response surface methodology (RSM), which presents an accurate prediction of the input-output relationship by considering parameter interactions [42]. Recently, the RSM has been employed to analyze and optimize the performance of various engineering systems including the Stirling engine [43,44]. Whereas, to the best of the authors' knowledge, no studies using RSM on Stirling regenerators have been reported to date, which provides another innovation for this paper.

Therefore, the main objective of this paper is to design and optimize a new annular regenerator for decreasing flow and axial heat conduction losses based on constructal concept and RSM. Different from the conventional porous regenerators of cross flows and the parallel geometry type regenerators of smooth flows, the matrix surface of the new regenerator was designed to be inclined to the gas flow direction for achieving a low flow resistance and relatively high heat transfer performance. The layered approach was applied to avoid contact between the matrix, thus minimizing the axial heat conduction. The bifurcation type structure, which has been proven to be an efficient configuration for obtaining excellent performance in constructal design, was used to design the regenerator to obtain a relatively uniform spatial distribution and a large heat transfer surface area of the matrix. After the design, the fluid flow and heat transfer mechanisms of the annular constructal bifurcation regenerator (CBR) were investigated. Thereafter, the response surface analysis was performed to quantify the relationship between the geometric parameters and regenerator performance. Based on the functions obtained by RSM, a multi-objective optimization of the regenerator structure was carried out using the Non-Dominated Sorting Genetic Algorithm II (NSGA-II). Finally, the overall performance of the CBR was compared with those of the porous regenerators and parallel geometry type regenerators.

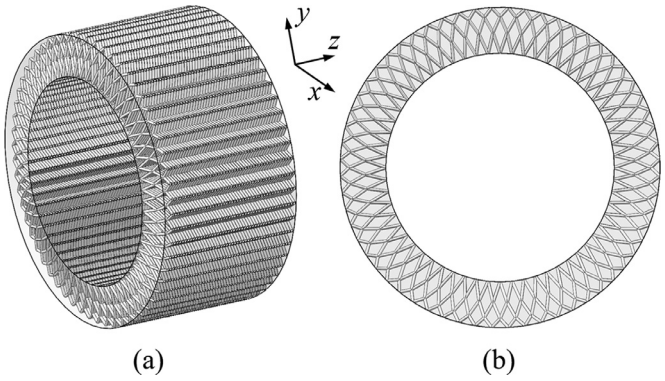

Fig. 1. Schematic of the whole CBR: (a) full view and (b) view from the z-direction.

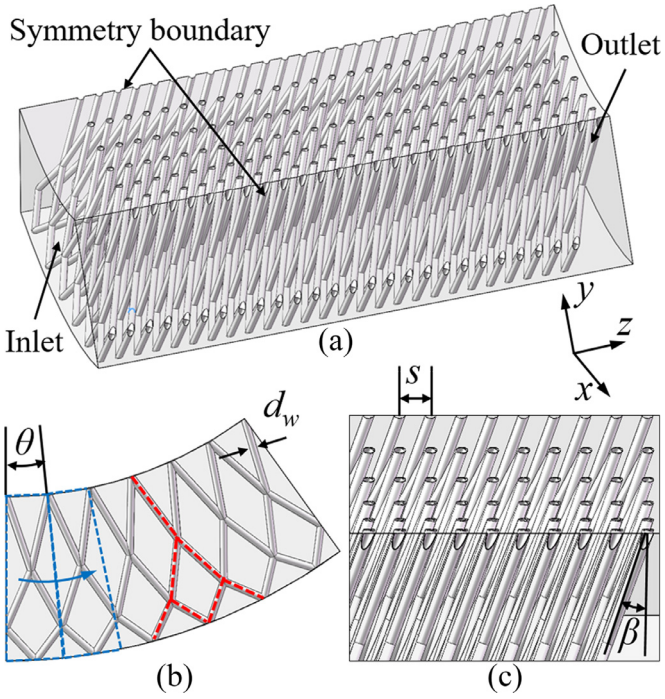

Fig. 2. Schematic of the computational domain for the CBR: (a) full view, (b) view from the z-direction, and (c) local view from the x-direction.

2. Physical model

The whole annular constructal bifurcation regenerator (CBR) designed based on the constructal concept is shown in Fig. 1. The CBR is composed of layers of wire mesh separated and aligned with each other. The contactless wire mesh is welded to two concentric thin wall metal cylinders for minimizing the axial conduction path of the regenerator. An inclined angle less than 90° is set between the wire mesh surface and the gas flow direction. The inner and outer diameters of the CBR (D_i and D_o) are 100 mm and 140 mm respectively, and the length L is 72 mm, which is in line with the size of the regenerator in practical application. Benefiting from the symmetry of the regenerator structure in the angular direction, one-tenth of the CBR is taken as the computational domain so as to save computing resources, as illustrated in Fig. 2(a). Fig. 2(b) and (c) are the views of the CBR from the z and x directions, respectively. As can be observed in Fig. 2(b), the design inspiration for the annular CBR comes from the two-level combination of bifurcation-shaped structures (marked with red lines). Adjacent bifurcation-shaped structures are superimposed on each other to form a matrix configuration analogous to the screen. Each

Table 1
Geometric parameters of the CBR.

Geometric parameter	Value
Regenerator length L (mm)	72
Regenerator outer diameter D_o (mm)	140
Regenerator inner diameter D_i (mm)	100
Wire mesh central angle θ (°)	6–18
Wire mesh inclined angle β (°)	10–30
Wire mesh pitch s (mm)	1.5–3.5
Wire diameter d_w (mm)	0.5–1.2

layer of wire mesh consists of numerous repeated structure units (marked with blue lines) with the same central angle θ. Except for the central angle θ, other main geometric parameters such as the inclined angle β, the pitch s, and the wire diameter d_w of the wire mesh are varied to study their effects on the performance of the CBR. The major geometric dimensions of the CBR are summarized in Table 1.

3. Numerical method

3.1. Governing equations

The gas flow in the regenerator is considered to be unsteady, viscous, and incompressible. During the regenerative process, the physical properties of the gas (helium) and solid (copper) are assumed to vary with temperature, and the effects of gravity, viscous heating, and radiative heat transfer are neglected. Based on the above assumptions, the governing equations are given as follows to describe the mass, momentum, and energy conservations in the CBR [45].

The mass conservation equation:

$$\frac{D\rho_f}{Dt} + \rho_f \nabla \cdot u = 0 \tag{1}$$

The momentum conservation equation:

$$\rho_f \frac{\partial u}{\partial t} + u \cdot \nabla(\rho_f u) = -\nabla p - \frac{2}{3}\nabla[\mu(\nabla \cdot u)] + \nabla \cdot \left[\mu(\nabla u + (\nabla u)^T)\right] \tag{2}$$

The energy conservation equation for the gas:

$$\rho_f c_{p,f} \frac{DT_f}{Dt} = \nabla \cdot (\lambda_f \nabla T_f) + \frac{Dp}{Dt} + h_l(T_s - T_f) \tag{3}$$

The energy conservation equation for the solid:

$$\rho_s c_{p,s} \frac{\partial T_s}{\partial t} = \nabla \cdot (\lambda_s \nabla T_s) + h_l(T_f - T_s) \tag{4}$$

In the above, t, μ, p, and $\boldsymbol{u}$ refer to the time, viscosity, pressure, and velocity vector, respectively; ρ_f, T_f, λ_f, and $c_{p,f}$ represent the density, temperature, thermal conductivity, and specific heat for the gas, respectively; and ρ_s, T_s, λ_s, and $c_{p,s}$ denote the density, temperature, thermal conductivity, and specific heat for the solid, respectively. Additionally, h_l is the tatal heat transfer coefficient at the interface between the gas and the matrix solid per unit length, which can be calculated as [9]:

$$h_l = a_r h \approx \frac{4(1-\gamma)}{d_w} h \tag{5}$$

where h is the convective heat transfer coefficient at the interface between the gas and the solid; a_r and γ mean the specific surface area and the porosity of the CBR, respectively. The porosity γ is determined as:

$$\gamma = 1 - \frac{V_s}{V} \tag{6}$$

where V and V_s denote the total volume and matrix solid volume for the CBR, respectively.

The convective heat transfer coefficient h is defined as:

$$h = \frac{q}{T_s - T_f} \tag{7}$$

where q is the heat flux at the interface between the gas and the solid.

In plenty of studies, the performance comparison of the regenerators with different structures is usually conducted under the same hydraulic Reynolds number Re_h defined as follows.

$$Re_h = \frac{u\rho_f d_h}{\mu} \tag{8}$$

where u is the bulk velocity of the gas in the CBR; d_h is the hydraulic diameter of the regenerator matrix, which can be calculated as [46]:

$$d_h = \frac{4\gamma V}{A_r} \approx \frac{\gamma d_w}{1-\gamma} \tag{9}$$

where A_r denotes the surface area of the matrix solid.

Generally, the criteria employed to evaluate the flow loss and heat transfer performance of the regenerator are the friction factor f_h and Nusselt number Nu_h based on the hydraulic diameter d_h, respectively:

$$f_h = \frac{2\Delta p d_h}{L\rho_f u^2} \tag{10}$$

$$Nu_h = \frac{h d_h}{\lambda_f} \tag{11}$$

where Δp represents the pressure drop of the gas at the inlet and outlet of the CBR.

However, the gas temperature in the regenerator is unpredictable before calculation, so the physical properties of the gas cannot be determined, thus it is difficult to choose appropriate boundary conditions to ensure that the regenerators with disparate geometric parameters are under the same hydraulic Reynolds number. As a result, this paper performs the performance evaluation of the CBR based on the same inlet Reynolds number Re_{in}, which is defined as:

$$Re_{in} = \frac{u_{in}\rho_{in}(D_o - D_i)}{\mu_{in}} \tag{12}$$

where u_{in}, ρ_{in}, and μ_{in} represent the velocity, density, and viscosity of the gas at the inlet of the CBR.

Since the CBRs with different geometric dimensions are not under the same hydraulic Reynolds number Re_h, it is unreasonable to apply Nusselt number Nu_h and friction factor f_h based on d_h to compare the flow and thermal performance of the CBRs with different dimension parameters. To reflect the effects of the geometric structures in the evaluation criterion, the dimensionless parameter NTU (the number of heat transfer units) is introduced here to characterize the transient thermal performance of the CBR, which is determined as [47]:

$$NTU = \frac{hA_r}{\dot{m}c_{p,f}} \tag{13}$$

where $\dot{m}$ is the mass flow rate of the gas.

Additionally, a global friction factor f is defined based on the overall dimension of the CBR to quantify the flow loss in the regenerator:

$$f = \frac{2\Delta p(D_o - D_i)}{L\rho_f u_{in}^2} \tag{14}$$

3.2. Solution procedure

The main boundary conditions of the CBR model are displayed in Fig. 2(a). In another study by the authors [36], the fluid flow and heat transfer characteristics at the maximum velocity of oscillating flows have been found to be nearly consistent with those of unidirectional flows in the regenerator. Hence, this paper simulates the regenerator in the unidirectional flow. In the numerical simulation, the values of operating conditions should be within a reasonable range, which is determined by the published experiments. Herein, at the regenerator inlet, a uniform velocity of 11 m/s (corresponding to inlet Reynold number Re_{in} = 10,000) and a constant temperature of 873 K are applied. At the regenerator outlet, a uniform pressure of 1.5 MPa is imposed. The values of these boundary conditions are selected within the range of experiments and consistent with the practical conditions. Moreover, symmetry boundary conditions are defined on the two axial sections of the regenerator. A no-slip coupled wall is supposed at the gas-solid interface to calculate the heat transfer between the gas and the solid. For the other surfaces, the no-slip adiabatic wall is assumed. In addition, the temperature of the gas and solid for the regenerator are initialized to constant values of 873 K and 673 K, respectively, yielding a temperature difference to enable heat transfer between the gas and solid.

Under the above boundary conditions, the flow pattern in the CBR is considered to be vigorously turbulent. Therefore, the RNG k-ε turbulence model is employed in this study due to its improving capabilities in predicting a highly swirling pattern and separation prevail flow compared with the standard k-ε turbulence model [48]. The pressure-based solver with double precision is applied to solve the governing equations. The coupled algorithm is selected to achieve the pressure-velocity coupling. The standard discretization scheme is used for the pressure term and the second order upwind discretization scheme is utilized for the momentum and energy terms. Additionally, the time step of the unsteady simulation is set to 0.0001 s, which is small enough to capture changes in the flow field and obtain good convergence. All the data in the paper are transient and obtained at the 200th time step.

3.3. Grid independence study

In this work, the commercial software ICEM 16.0 is applied to generate grid systems of the regenerator model. Unstructured grids are used in the whole CBR owing to the complex structures of the regenerator. To ensure the accuracy of the numerical simulation, a grid independence study is carried out at $\theta = 6°$, $\beta = 10°$, $s = 1.5$ mm, and $d_w = 1.2$ mm. The global friction factor f and the number of heat transfer units NTU for three grid systems with different grid numbers 7133000, 12357000, and 19521000 are tested and compared, as shown in Fig. 3. The results indicate that the grid system with 12357000 grid elements satisfies the independence requirement as the deviations of f and NTU are 2.6% and 1.8% respectively compared with the grid system with 19521000 grid elements.

3.4. Model validation

In the open published literature, there is no experimental data related to the new CBR developed in the present study. In addition, it is hard to fabricate and test the CBR at present on account of the complexity of its structures. Therefore, the traditional woven screen regenerator commonly used in Stirling engines is employed to validate the accuracy of the numerical method proposed in this paper due to its similar wire mesh structures with the CBR. Herein, a detailed 3-D model for a representative differential part of the misaligned stacked woven screen regenerator matrix is established.

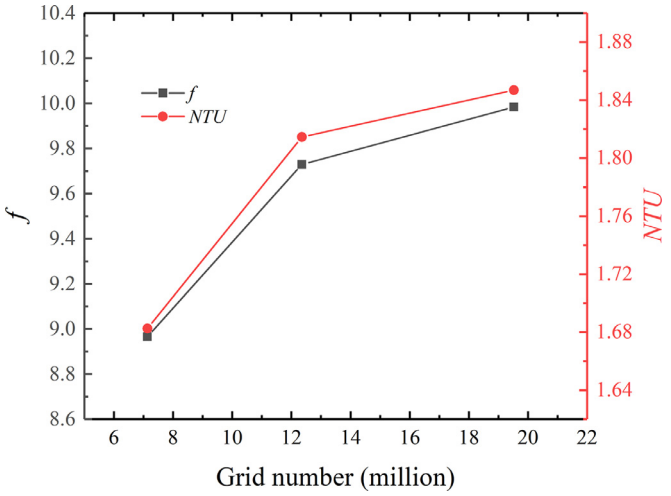

Fig. 3. Grid independence tests of the CBR.

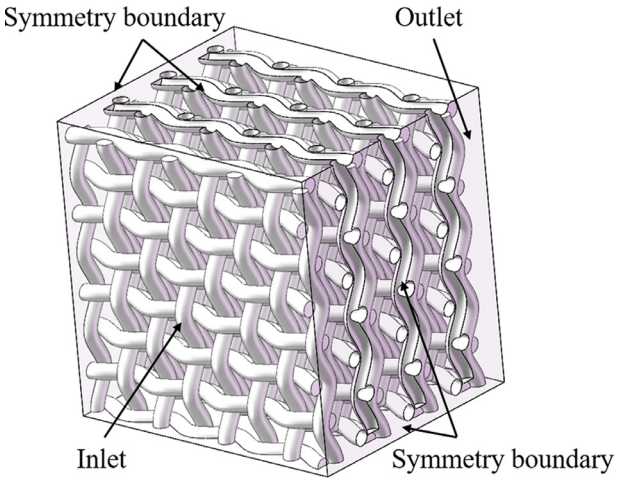

Fig. 4. Structures and boundary conditions of the miniature woven screen regenerator matrix model.

The structures and boundary conditions of the miniature regenerator matrix are illustrated in Fig. 4. A numerical simulation of the regenerator matrix model is performed using the same numerical scheme to investigate the flow resistance and heat transfer characteristics in the regenerator. The numerical results are compared with the empirical correlations presented by Tanaka et al. [15] and Gedeon and Wood [16]. The dimension parameters of the miniature regenerator matrix model built in this work and the regenerators experimentally studied by Tanaka et al. and Gedeon et al. are listed in Table 2. It can be observed that the dimensions of the regenerator matrix model are almost within the experimental ranges. Therefore, the empirical correlations developed by the experimental works can be applied to the woven screen regenerator matrix model presented in this study.

The friction factor f_h and Nusselt number Nu_h obtained from the numerical simulation and experiments are compared, as shown in Fig. 5. According to Fig. 5(a), it is clear that the f_h from the simulation agrees well with the correlations of Gedeon and Wood, with a deviation limited to 12.9%. Fig. 5(b) illustrates that numerical Nu_h is almost consistent with the correlations of Tanaka et al. as the maximum deviation between them is 5.9%. Considering the uncertainty of the experiment and the geometric difference between the established numerical model and the actual matrix, the error of the numerical simulation is within the acceptable range. Therefore,

Table 2
Dimensions of the woven screen regenerator matrix built in this study and tested by Tanaka et al. and Gedeon and Wood.

	Mesh number	Wire diameter (mm)	Porosity	Model size (mm^3)
Present study	100	0.1	0.733	$1.905^2 \times 1.54$
Tanaka et al.	50–200	0.05–0.23	0.645–0.754	-
Gedeon and Wood	80–200	0.053–0.094	0.623–0.781	-

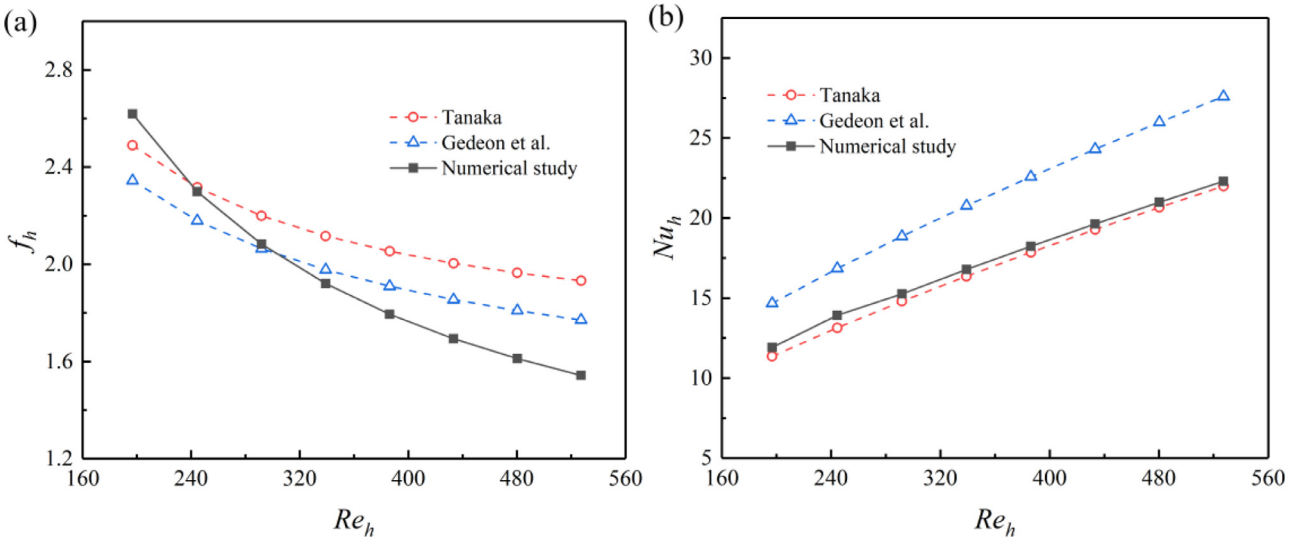

Fig. 5. Comparison between the numerical results and the experimental correlations for the woven screen regenerator matrix: (a) f_h and (b) Nu_h.

Table 3
Input variables and their three levels.

Variable	Level		
	-1	0	1
Central angle θ (A), °	6	12	18
Inclined angle β (B), °	10	20	30
Pitch s (C), mm	1.5	2.5	3.5
Wire diameter d_w (D), mm	0.5	0.85	1.2

it can be considered that the numerical method presented in this study is reliable and accurate.

4. Response surface methodology (RSM)

In this study, the response surface methodology (RSM) is applied to establish the functional relationship between design variables and objective responses and to analyze the interactive effects of different variables on the responses based on the data obtained from the previous numerical simulation. Note that the main geometric parameters of the CBR including the central angle θ (A), the inclined angle β (B), the pitch s (C), and the wire diameter d_w (D) of the wire mesh are selected as the input variables, and the global friction factor f and the number of heat transfer units NTU are chosen as the output responses. The central composite design (CCD) proposed by Box and Wilson is employed to design the numerical experiment. It is assumed that each variable has three levels. The input variables and their levels are summarized in Table 3.

In the response surface analysis, the quadratic polynomial regression model is usually used to approximate the functional relationship. The general form of the model can be expressed as:

$$Y = \alpha_0 + \sum_{i=1}^{n} \alpha_i x_i + \sum_{i=1}^{n-1} \sum_{j=i+1}^{n} \alpha_{ij} x_i x_j + \sum_{i=1}^{n} \alpha_{ii} x_i^2 + e \quad (15)$$

where Y is the objective response; x_i and x_j represent the design variables; n represents the number of the design variables; α_0, α_i, α_{ij}, and α_{ii} denote the regression coefficients of the model; e denotes the statistical error.

The CCD requires$2^n + 2n + b$runs to complete the design of experiments (DOE), where b represents the number center points. In this paper, 4 variables and 6 center points are included, so 30 runs are required for the DOE. The detailed information of all the runs in the DOE including the variable values and the response results are presented in Table 4.

5. Results and discussion

5.1. Analysis of flow and heat transfer in the regenerator

To understand the flow and heat transfer mechanisms in the new CBR and the causes for performance difference of the regenerator with different geometric parameters, there is a need to analyze and compare the physical fields in the regenerator. Five cases of regenerators in the DOE are selected as representatives to investigate the effects of the structures. The detailed information of the five regenerators are listed in Table 5. It can be observed that each of the cases II-V differs from the case I in only one geometric parameter, while the others remain the same.

Fig. 6(a) presents the streamline colored by velocity magnitude at the cross-section of the CBR for the cases II and V. From a macroscopic point of view, the repeatability of the regenerator structure units in the circumferential direction leads to a relatively uniform distribution of the whole matrix in space, which further results in a comparatively even spatial profile of the gas in the entire regenerator, thus facilitating the sufficient contact and heat transfer between the gas and the matrix. From a local perspective, a number of small pseudo-channels are formatted in the regenerator due to the regular matrix structures. The gas is relatively concentrated in these small pseudo-channels, which is simi-

Table 4
Design of experiments.

Run order	Real value			Response			Run order	Real value			Response		
	θ	β	s	d_w	f	NTU		θ	β	s	d_w	f	NTU
1	6	30	1.5	0.5	2.982	0.6660	16	6	30	3.5	0.5	2.048	0.2579
2	12	20	2.5	0.85	2.241	0.4040	17	6	30	1.5	1.2	5.416	1.643
3	12	20	2.5	1.2	3.778	0.6355	18	6	20	2.5	0.85	4.618	0.7958
4	12	20	2.5	0.85	2.241	0.4040	19	12	20	2.5	0.5	1.448	0.2279
5	6	10	3.5	1.2	8.041	0.8346	20	6	10	1.5	0.5	3.641	0.5821
6	18	10	1.5	0.5	1.398	0.2558	21	12	20	2.5	0.85	2.241	0.4040
7	18	10	1.5	1.2	2.402	0.7847	22	6	30	3.5	1.2	5.778	0.8150
8	18	30	1.5	1.2	1.760	0.7096	23	12	20	2.5	0.85	2.241	0.4040
9	18	30	3.5	0.5	0.8886	0.1127	24	18	10	3.5	1.2	2.331	0.3700
10	18	20	2.5	0.85	1.659	0.3371	25	12	20	2.5	0.85	2.241	0.4040
11	12	20	3.5	0.85	2.008	0.3006	26	6	10	3.5	0.5	2.858	0.2728
12	12	20	1.5	0.85	2.565	0.6561	27	18	30	3.5	1.2	2.012	0.3405
13	12	20	2.5	0.85	2.241	0.4040	28	12	30	2.5	0.85	2.072	0.3951
14	18	10	3.5	0.5	1.074	0.1572	29	18	30	1.5	0.5	1.196	0.2528
15	6	10	1.5	1.2	9.729	1.815	30	12	10	2.5	0.85	2.165	0.4064

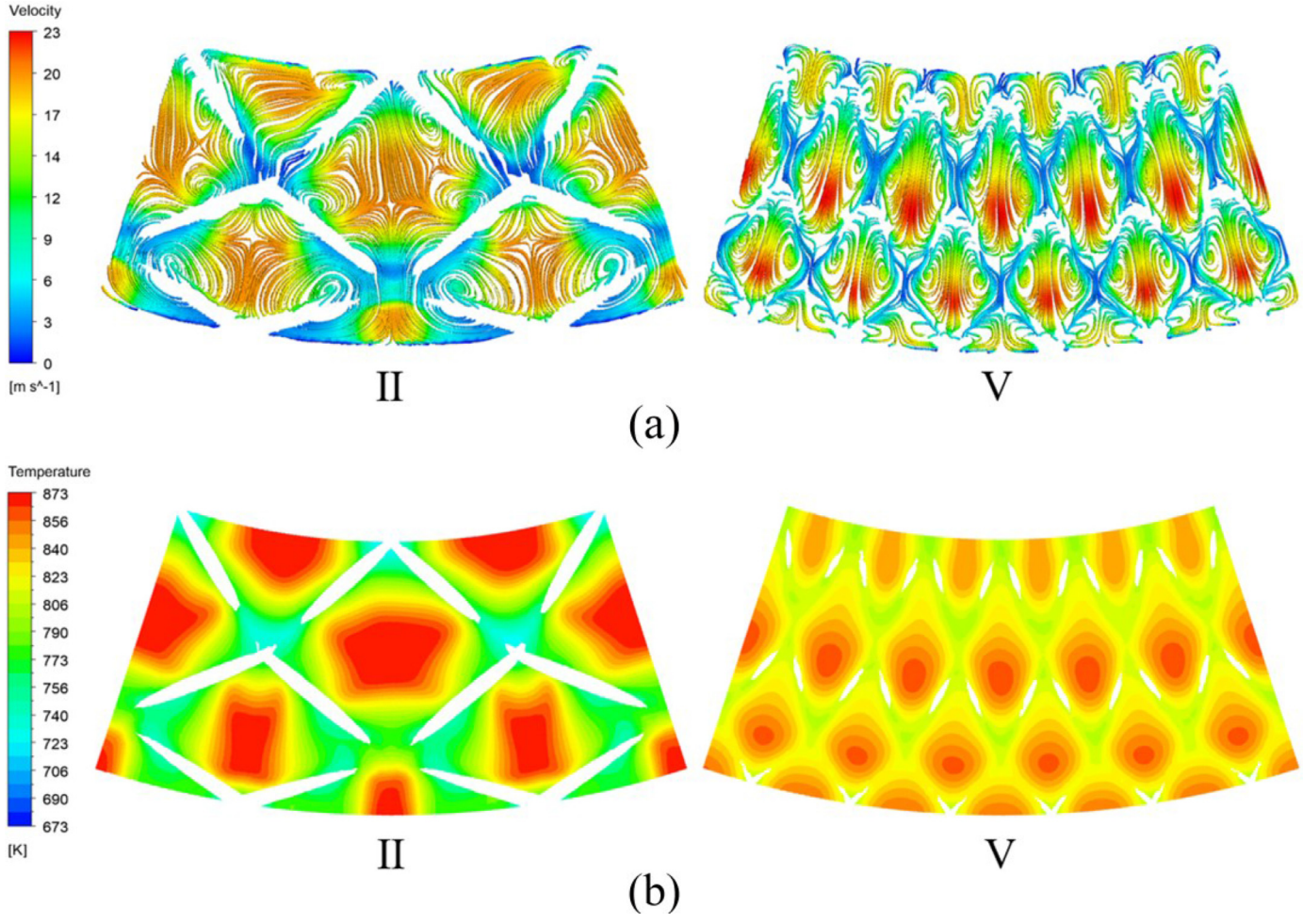

Fig. 6. Physical fields at the middle cross-section of the CBR: (a) 2-D streamline colored by velocity magnitude and (b) temperature.

lar to the core flow in the actual channel, so that the flow loss in the regenerator can be significantly decreased. Additionally, multitudinous local vortex structures are formed in the flow, intensifying the collision between the gas and the matrix and accelerating the gas mixing effectively. This will evidently reduce the average gas temperature and increase the temperature gradient of the gas near the matrix solid, thus enhancing the thermal performance of the regenerator, which is reflected in the temperature contours in Fig. 6(b).

The physical fields at the axial section of the five regenerators are drawn and compared in Fig. 7. As illustrated in Fig. 7(a), it is clear that a consecutive flow resembling the core flow in the channels is formed in the regenerator due to the existence of the pseudo-channels, which is consistent with that shown in Fig. 6. Therefore, an extremely low pressure drop is generated in the regenerator, with being limited to 1000 Pa for most of the CBR and much lower than that of the conventional porous regenerators, as shown in Fig. 7(b). Fig. 7(c) presents the temperature profiles at

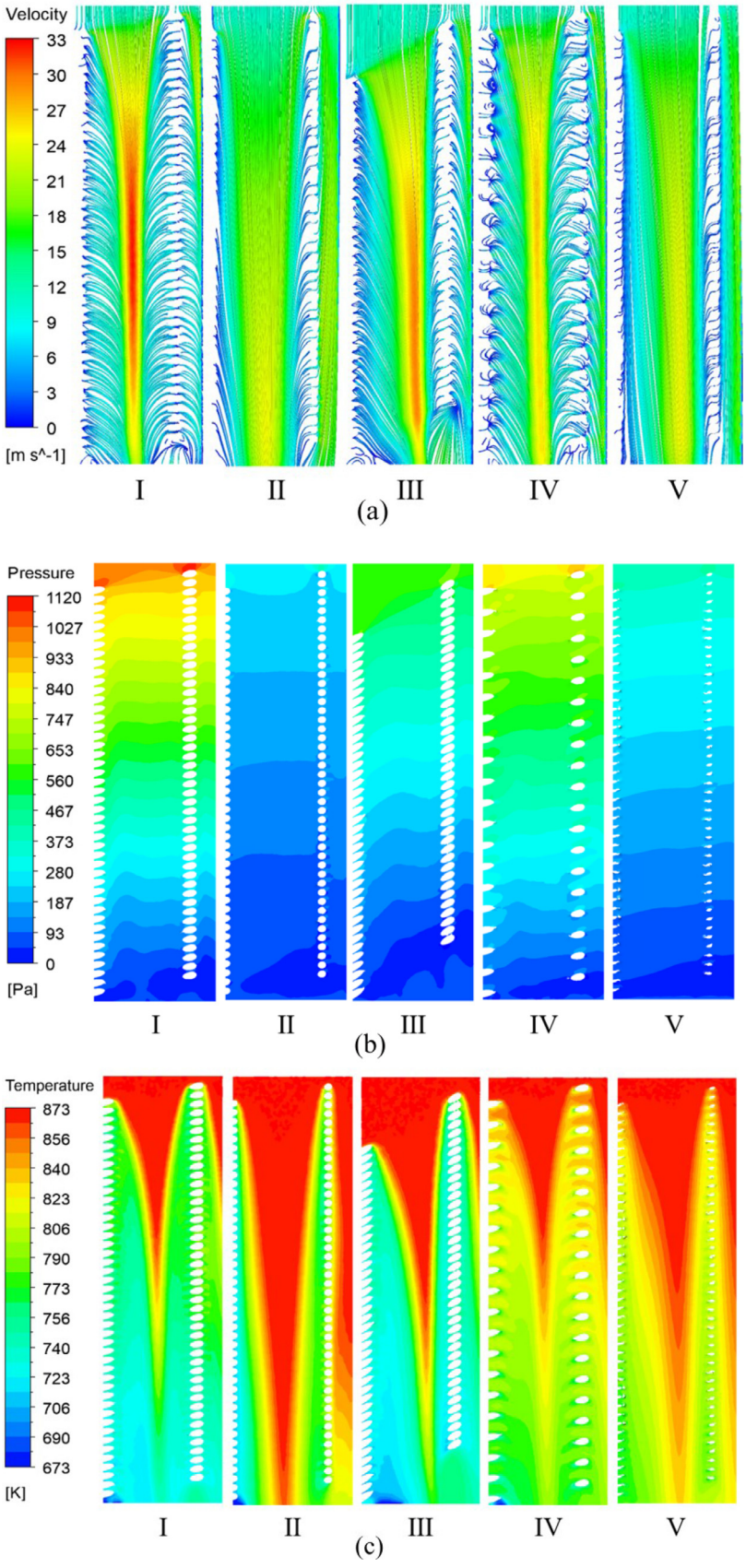

Fig. 7. Physical fields at the axial section of the CBR: (a) 2-D streamline colored by velocity magnitude, (b) pressure, and (c) temperature.

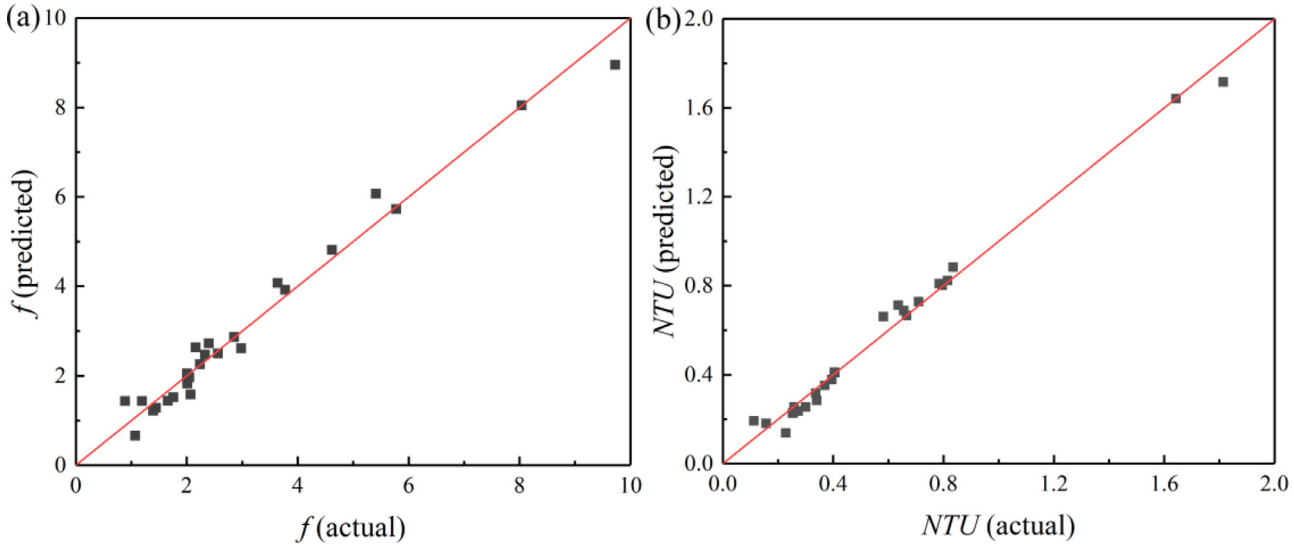

Fig. 8. Comparison between the actual numerical values and the predicted values: (a) f and (b) NTU.

Table 5
Information of the five regenerator cases selected from the DOE.

Number	Run order	θ	β	s	d_w	f	NTU
I	15	6	10	1.5	1.2	9.729	1.815
II	7	18	10	1.5	1.2	2.402	0.7847
III	17	6	30	1.5	1.2	5.416	1.643
IV	5	6	10	3.5	1.2	8.041	0.8346
V	20	6	10	1.5	0.5	3.641	0.5821

Table 6
ANOVA for *f*.

Source	Sum of squares	DF	Mean square	F-value	*p*-value
Model	113.53	14	8.11	44.32	0.0000
Linear					
A	51.31	1	51.31	280.44	0.0000
B	5.00	1	5.00	27.32	0.0000
C	0.9117	1	0.9117	4.98	0.0413
D	31.24	1	31.24	170.74	0.0000
Interaction					
AB	2.80	1	2.80	15.31	0.0014
AC	0.4203	1	0.4203	2.30	0.1504
AD	11.37	1	11.37	62.14	0.0000
BC	0.3133	1	0.3111	1.71	0.2104
BD	2.02	1	2.02	11.03	0.0047
CD	0.0908	1	0.0908	0.4963	0.4919
Square					
A^2	1.98	1	1.98	10.81	0.0050
B^2	0.0558	1	0.0558	0.3048	0.5890
C^2	0.0011	1	0.0011	0.0062	0.9382
D^2	0.3129	1	0.3129	1.71	0.2106
Residual	2.74	15	0.1830	-	-
Lack of Fit	2.74	10	0.2744	-	-
Pure Error	0.0000	5	0.0000	-	-
Cor Total	116.27	29	-	-	-

R^2 = 0.9764, R^2 (Adjusted) = 0.9544, Adeq Precision = 27.4045.

the axial section of the CBR. When the gas flows into the regenerator from the hot end, the temperature of the gas drops rapidly because of its strong interaction with the cold matrix. In addition, it can be observed that the structure parameters have a significant effect on the flow and thermal performance of the CBR. Generally, the regenerator with lower flow resistance offers better heat transfer performance. The specific effects of different geometric parameters on the physical mechanisms in the regenerator will be expounded in detail in combination with RSM analysis later.

Table 7
ANOVA for *NTU*.

Source	Sum of squares	DF	Mean square	F-value	*p*-value
Model	4.20	14	0.3003	89.52	0.0000
Linear					
A	1.06	1	1.06	314.97	0.0000
B	0.0045	1	0.0045	1.35	0.2634
C	0.8465	1	0.8465	252.32	0.0000
D	1.48	1	1.48	441.31	0.0000
Interaction					
AB	0.0001	1	0.0001	0.0166	0.8992
AC	0.1412	1	0.1412	42.09	0.0000
AD	0.2261	1	0.2261	67.41	0.0000
BC	0.0002	1	0.0002	0.0615	0.8075
BD	0.0063	1	0.0063	1.88	0.1910
CD	0.1672	1	0.1672	49.85	0.0000
Square					
A^2	0.0574	1	0.0574	17.11	0.0009
B^2	0.0007	1	0.0007	0.2184	0.6470
C^2	0.0096	1	0.0096	2.85	0.1118
D^2	0.0005	1	0.0005	0.1533	0.7009
Residual	0.0503	15	0.0034	-	-
Lack of Fit	0.0503	10	0.0050	-	-
Pure Error	0.0000	5	0.0000	-	-
Cor Total	4.25	29	-	-	-

R^2 = 0.9882, R^2 (Adjusted) = 0.9771, Adeq Precision = 38.5296.

5.2. Analysis of variance (ANOVA) and RSM analysis for interactive effects of geometric parameters

5.2.1. ANOVA analysis

The quadratic polynomial regression models representing the functional relationships for the global friction factor f and the number of heat transfer units NTU are obtained from the RSM as follows:

$$\begin{aligned} f = {} & 6.957 - 0.7296A - 0.02644B - 1.117C + 5.249D \\ & + 0.006974AB + 0.02701AC - 0.4014AD \\ & + 0.01399BC - 0.1015BD + 0.2152CD + 0.02427A^2 \\ & - 0.001467B^2 + 0.02096C^2 + 2.8371D^2 \end{aligned} \tag{16}$$

$$\begin{aligned} NTU = {} & 0.9496 - 0.1300A + 0.009430B - 0.4676C + 2.147D \\ & - 0.000031AB + 0.01566AC - 0.05661AD \\ & + 0.000359BC - 0.005665BD - 0.2921CD + 0.004134A^2 \\ & - 0.000168B^2 + 0.06079C^2 + 0.1150D^2 \end{aligned} \tag{17}$$

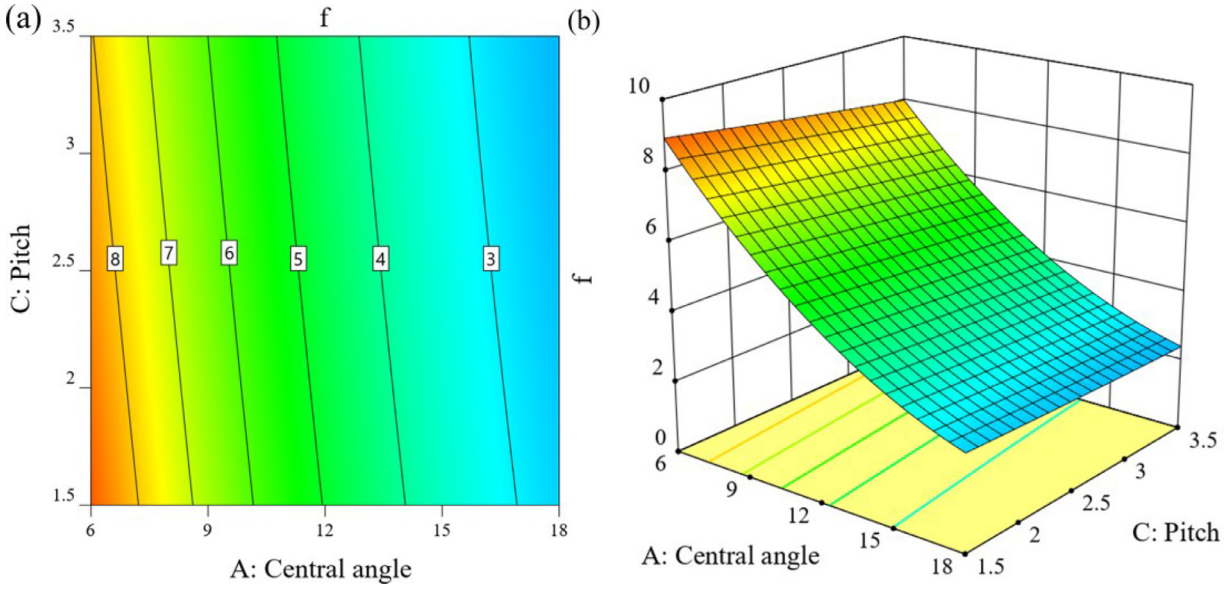

Fig. 9. Interactive effects of the central angle θ and wire mesh pitch s on the f: (a) 2-D contour plot and (b) 3-D surface plot.

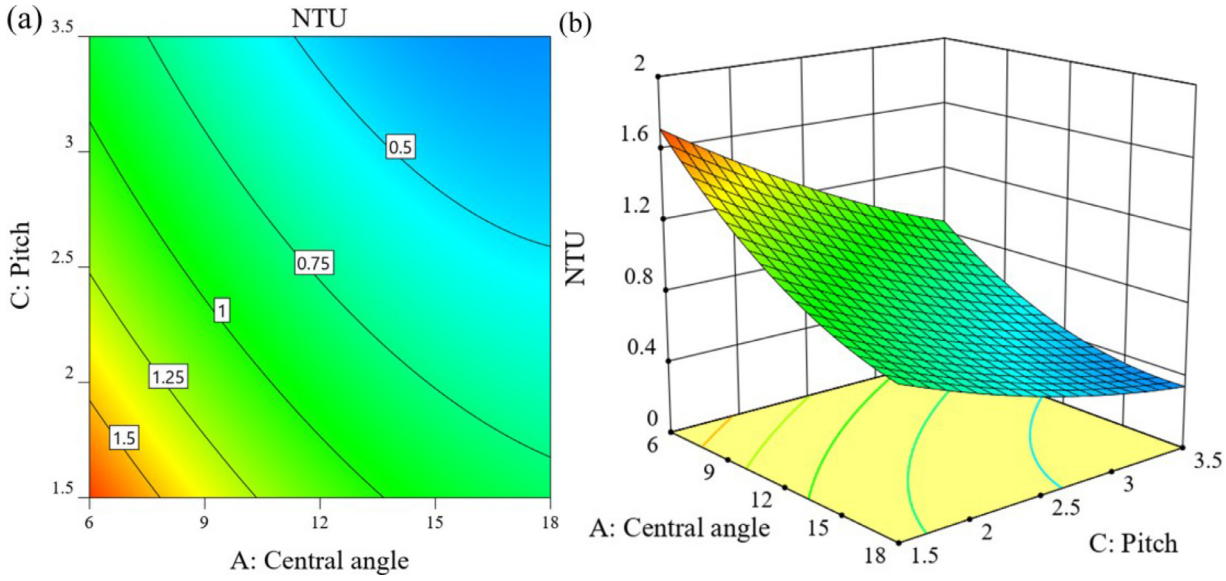

Fig. 10. Interactive effects of the central angle θ and wire mesh pitch s on the NTU: (a) 2-D contour plot and (b) 3-D surface plot.

To evaluate the adequacy and significance of the models, the analysis of variance (ANOVA) is conducted, whose results are presented in Tables 6 and 7. In ANOVA, the sum of squares represents the deviation of each variable from the population mean. The mean square is calculated by dividing the sum of squares by the degrees of freedom (DF). The F-value is constructed as the ratio of the mean square for each model term to the mean square for the residual. An F-value higher than the critical value should be obtained to ensure the sufficient significance of the model term. The p-value is defined as the minimum level of significance test for rejecting the null hypothesis. In this paper, a p-value less than 0.05 means a significant effect of the selected model term on the responses. In addition, R^2 is used to measure the goodness of fit for the regression model, and an R^2 value closer to 1 indicates that the model fits the observed data better. The Adjusted R^2 is modified from the R^2 after considering the effects of the numbers of the total samples and design variables. The Adeq Precision is a criterion for evaluating the signal to noise ratio, which is advisable when greater than 4.

Table 6 shows the ANOVA results for the global friction factor *f*. The F-value of the whole regression model is 44.32, which implies that the model is significant. The values of R^2 and Adjusted R^2 are 0.9764 and 0.9544, respectively, and the Adeq Precision gives a high value of 27.4045, indicating that the model has a high accuracy for approximating the functional relationship. Besides, in the aspects of the individual model term, the terms A, B, C, D, AB, AD, BD, and A^2 have significant effects on the global friction factor *f* due to the p-values of them are lower than 0.05.

The ANOVA results for the number of heat transfer units *NTU* is shown in Table 7. It can be seen that the regression model offers an adequate significance with the F-value of the model being equal to 89.52. Additionally, the values for R^2, Adjusted R^2, and Adeq Precision are 0.9882, 0.9771, and 38.5296, respectively. It demonstrates that the model provides a high goodness of fit for the ob-

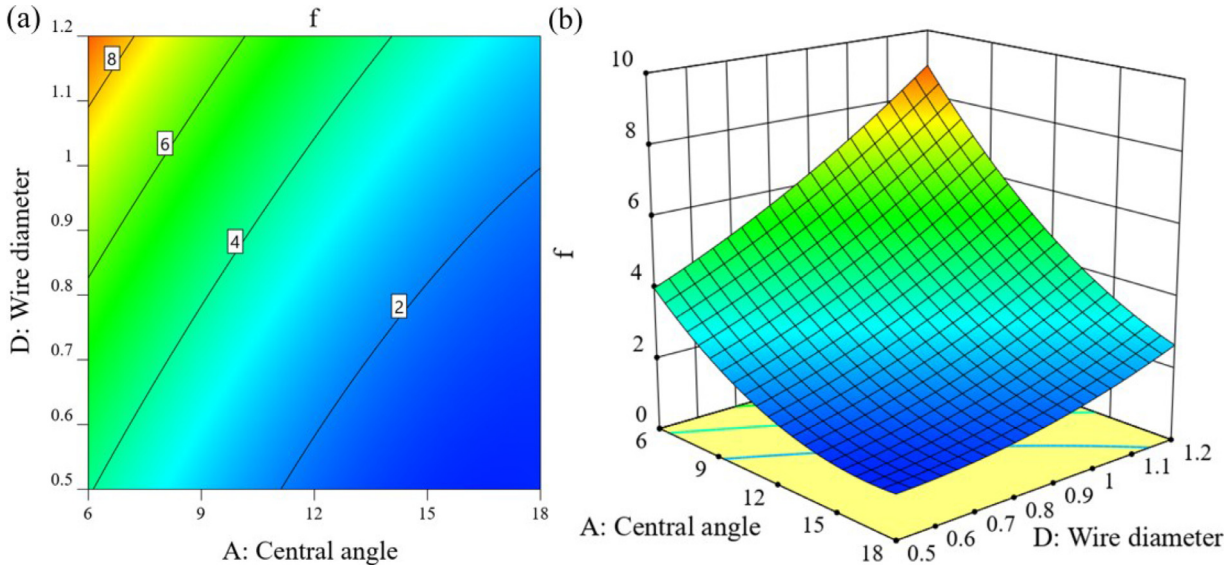

Fig. 11. Interactive effects of the central angle θ and wire diameter d_w on the f: (a) 2-D contour plot and (b) 3-D surface plot.

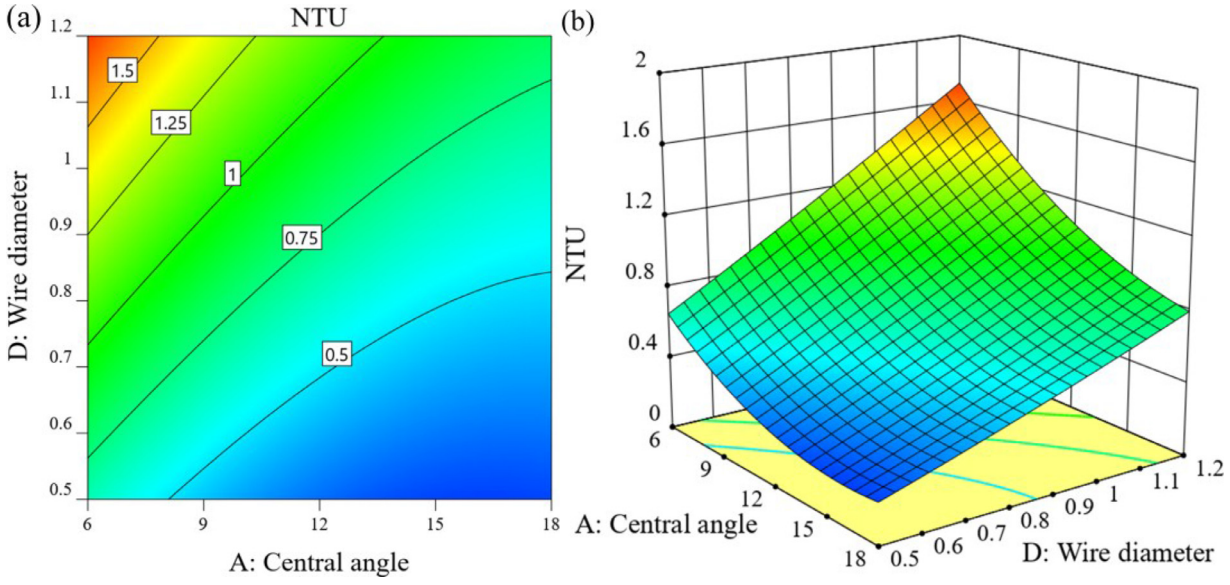

Fig. 12. Interactive effects of the central angle θ and wire diameter d_w on the NTU: (a) 2-D contour plot and (b) 3-D surface plot.

tained numerical data. According to the p-value less than 0.05, the model terms A, C, D, AC, AD, CD, and A^2 are the significant terms for the *NTU*.

To further validate the accuracy of the quadratic polynomial regression models, comparisons between the actual numerical values and the predicted values for the objective responses are carried out and shown in Fig. 8. It is clear that the points are uniformly distributed around the diagonal line, with the average deviations between the predicted values and the actual values being 9.7% and 8.2% for the *f* and *NTU*, respectively. Therefore, combined with the above ANOVA analysis, it can be considered that the regression model presented in this paper is sufficiently accurate to predict the performance of the regenerator.

5.2.2. RSM analysis for interactive effects of geometric parameters

The 2-D and 3-D response surface plots are drawn to analyze the interactive effects of the geometric parameters on the performance of the CBR, as illustrated in Figs. 9–14. Figs. 9 and 10 present the combined effects of the central angle θ and wire mesh pitch *s* on the global friction factor *f* and the number of heat transfer units *NTU*. It can be seen that both flow loss and thermal performance decrease significantly with the rise of the central angle. The causes of this phenomenon can be found by comparing Fig. 7 I and II. As the central angle raises, the hydraulic diameter of the pseudo-channel in the regenerator increases, so more gas flows directly through the center of the channel, which will reduce the interaction between the gas and the matrix, thus leading to the decrease of the flow resistance and the heat transfer rate. Besides, the effects of the wire mesh pitch on the thermal performance are similar to those of the central angle. However, the flow loss decreases slightly as the wire mesh pitch increases. With the increase of the pitch, the volume and surface area of the matrix decrease correspondingly, resulting in a reduction of the heat transfer between the gas and the matrix. At the same time, the decrease of the matrix surface area will also yield a lower viscous resistance on the matrix surface. Nevertheless, as the pitch raises, the combined influence of two adjacent layers of matrix wire mesh on the gas flow between them seems to become greater, and even

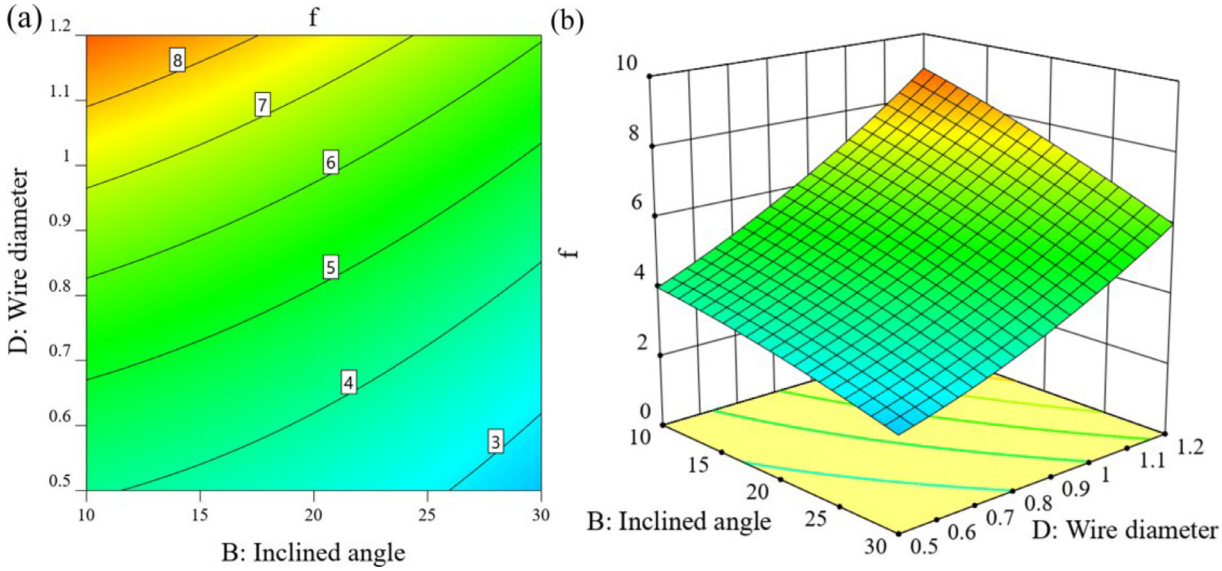

Fig. 13. Interactive effects of the inclined angle β and the wire diameter d_w on the f: (a) 2-D contour plot and (b) 3-D surface plot.

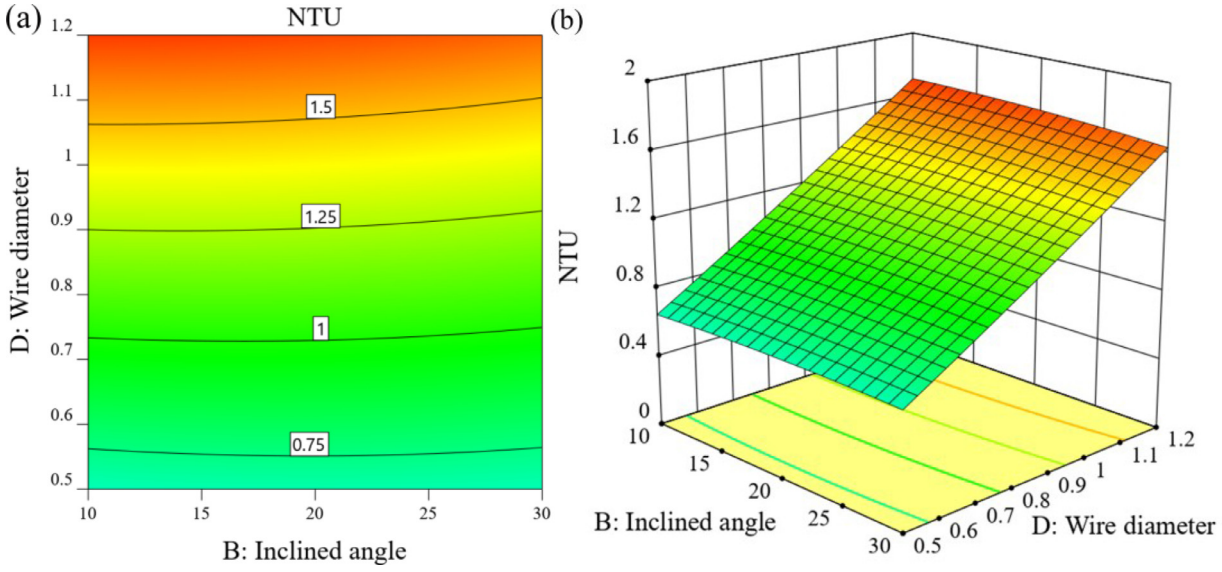

Fig. 14. Interactive effects of the inclined angle β and the wire diameter d_w on the NTU: (a) 2-D contour plot and (b) 3-D surface plot.

an obvious swirling flow is formed in the gap between the two adjacent layers of wire mesh, as illustrated in Fig. 7 I and IV. This phenomenon will bring about an increase in the inertial resistance of the gas. Hence, the opposite variations of these two kinds of flow resistance result in a slow change of the total flow loss.

Figs. 11 and 12 show the interactive effects of the central angle θ and the wire diameter d_w on the flow loss and thermal performance of the regenerator. It is clear that the regenerator with the larger wire diameter has a higher flow loss and thermal performance. This phenomenon can be explained by analyzing Fig. 7 I and V. Compared with the case I, the matrix of the case V with a smaller wire diameter shows an inconspicuous influence on the gas flow due to the decreasing windward surface area of the matrix to the gas, which leads to a decrease in flow resistance and heat transfer performance. This effect seems to be similar to that of the raise of the central angle. Additionally, it can be observed that at a smaller central angle, the effects of the wire diameter on the overall performance of the regenerator are more significant.

The interactive effects of the inclined angle β and the wire diameter d_w on the flow and heat transfer characteristics for the CBR are illustrated in Figs. 13 and 14. Fig. 13 shows that the flow loss in the regenerator decreases evidently with the rise of the inclined angle, which is consistent with the original intention of the design in this paper. According to Fig. 7 I and III, as the inclined angle increases, a higher axial velocity component is retained after the gas impinges on the matrix, so that less mechanical energy of the gas is consumed in the flow. In Fig. 14, the thermal performance of the regenerator appears to vary inappreciably with the inclined angle. However, note that with the increase of the inclined angle, the reduction of the thermal performance becomes more apparent. Therefore, it is reasonable to consider that the heat transfer of the regenerator changes slightly only in the relatively narrow range of the inclined angle studied in this paper, while with the further increase of the inclined angle, the heat transfer may be significantly reduced. As a result, a more extensive range of inclined angles is required to fully explore the effects of the inclined angle on the thermal performance of the CBR in a future study.

Table 8
Parameter settings of the NSGA-II.

Parameter	Value setting
Population size	300
Generation	1000
Pareto fraction	0.3
Crossover fraction	0.8
Function tolerance	10^{-5}

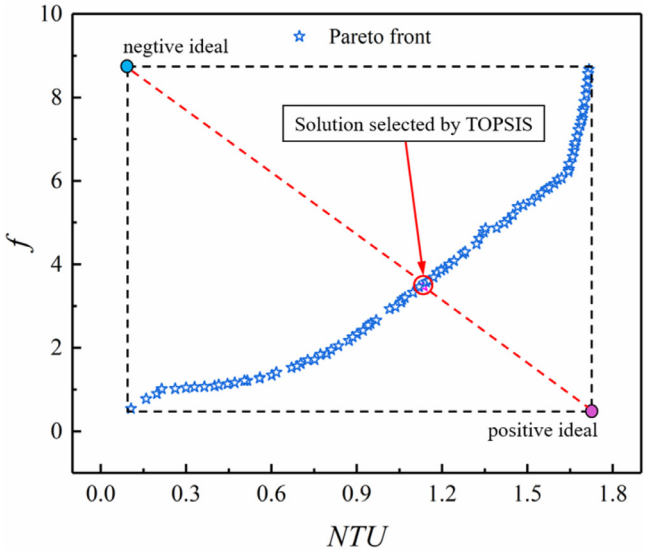

Fig. 15. Pareto front and the optimal solution selected by TOPSIS.

5.3. Multi-objective optimization

An ideal regenerator should have the best thermal performance and the lowest flow resistance. However, according to the response surface analysis above, for CBRs with different geometric parameters, an excellent heat transfer performance is always accompanied by a high flow loss. To achieve the optimal combination of these two conflicting objectives, a multi-objective optimization is performed based on the objective functions obtained from the RSM analysis. The objective functions and constraints in the optimization are given as:

$$\text{Minimization}: \ f = f_1(\theta, \beta, s, d_w);$$
$$\text{Maximization}: NTU = f_2(\theta, \beta, s, d_w);$$
$$\text{Subjected to}: \theta \in [6^\circ, 18^\circ], \ \beta \in [10^\circ, 30^\circ],$$
$$s \in [1.5\text{mm}, 3.5\text{mm}], \ d_w \in [0.5\text{mm}, 1.2\text{mm}],$$

In the present paper, the fast non-dominated sorting genetic algorithm (NSGA-II) embedded in the *gamultiobj* toolbox of Matlab is employed for the optimization of the objectives. The main parameter settings of the NSGA-II are presented in Table 8. Fig. 15 shows the optimal Pareto front obtained by the NSGA-II. All the solutions on the Pareto front are optimal that no one is superior to any other. To determine the most eclectic solution for practical applications, Technique for Order Preference by Similarity to Ideal Solution (TOPSIS) is selected as the decision-making method. An optimal solution is gained according to the TOPSIS method, as illustrated in Fig. 15. In this solution, the optimal combination of the geometric dimensions is $\theta = 10.91^\circ$, $\beta = 29.25^\circ$, $s = 1.512$ mm, and $d_w = 1.197$ mm. The f and the NTU of the selected optimal solution are 3.478 and 1.135, respectively. Compared to the extreme solution with the maximum NTU, the f at the selected optimal solution decreases 59.9%, while the NTU reduces only 33.9%. Analogously, compared to the extreme solution with the minimum f, the selected solution increases 9.68 times in NTU while only 5.42 times in f. Therefore, it can be considered that the optimal solution de-

Table 9
Conditions ranges of the three types of regenerators used for comparisons.

	Regenerator type	Re_h	Porosity	Wire or channel diameter (mm)
Tanaka et al.	woven screen regenerator	10–2000	0.645–0.754	0.05–0.23
Alfarawi et al.	miniature-channel regenerator	100–1400	0.248–0.433	0.4–1.5
Present study	annular constructal bifurcation regenerator	1580–15100	0.767–0.98	0.5–1.2

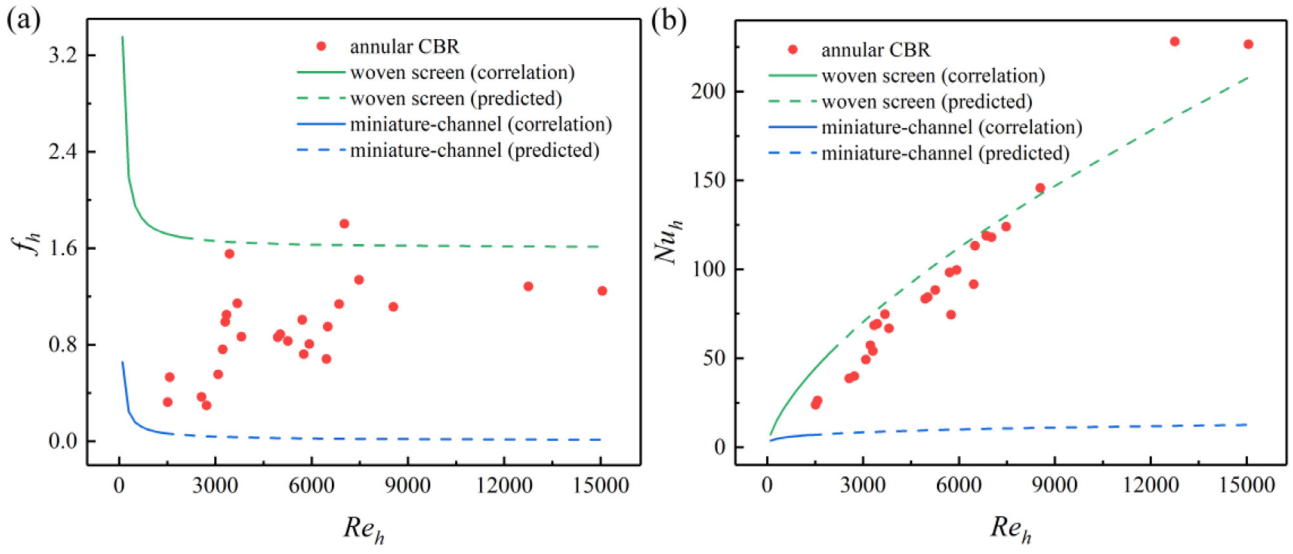

Fig. 16. Performance comparison of different types of regenerators: (a) f_h and (b) Nu_h.

termined by the TOPSIS method presents an excellent performance within the range of studied geometric parameters.

5.4. Comparison with the porous regenerators and parallel geometry type regenerators

In this section, a comparison of the flow resistance and thermal performance for the annular CBR with those of the conventional porous regenerators and parallel geometry type regenerators is carried out to evaluate the effectiveness of the CBR. The commonly used woven screen regenerators [15] and miniature-channel regenerators [27] are selected as the representatives of the porous regenerators and parallel geometry type regenerators, respectively. The condition ranges of these two types of regenerators and the CBR are listed in Table 9. To ensure the comparison is reasonable, the friction factor f_h and Nusselt number Nu_h based on the hydraulic diameter d_h are used to characterize the different types of regenerators. Fig. 16 presents the results of the comparison. Due to the substantial difference of the hydraulic Reynolds number Re_h between the literature and this study, the f_h and the Nu_h of the woven screen regenerators and miniature-channel regenerators are predicted in a larger Re_h range according to the experimental or numerical correlations. As expected, it is clear that the flow resistance of the CBR is between the woven screen regenerators and the miniature-channel regenerators. In addition, the heat transfer performance of the CBR is slightly lower than that of the woven screen regenerators, while significantly higher than that of the miniature-channel regenerators. Consequently, it can be proved that compared with the most commonly used porous regenerators currently, the CBR evidently reduces the flow loss, meanwhile avoids the deterioration of heat transfer performance.

6. Conclusion

In this paper, a new annular constructal bifurcation regenerator (CBR) was designed to reduce the fluid flow and axial heat conduction losses in the regenerator of Stirling engines based on the constructal concept. The flow and heat transfer characteristics of the CBRs with different geometry parameters were investigated and compared using the numerical simulation and the response surface methodology (RSM). The following conclusions can be drawn:

1. Due to the existence of inclined wire mesh and numerous pseudo-channels, a consecutive core flow with a large axial velocity component is formed in the CBR, thus substantially reducing the flow loss of the regenerator. Additionally, multitudinous local eddy structures are generated in the flow, which effectively intensifies the shock of the gas on the matrix solid and accelerates the gas mixing, so that the thermal performance of the regenerator will be significantly enhanced.
2. The quadratic polynomial regression models between the geometric parameters and the regenerator performance were established using RSM based on the data obtained by numerical simulation. The ANOVA analysis has demonstrated that the current regression models have sufficient significance and accuracy, with the deviations between the predicted values and the actual values being 9.7% and 8.2% for the f and NTU, respectively.
3. The dimension parameters such as the central angle θ, the inclined angle β, the pitch s, and the wire diameter d_w of the wire mesh have a powerful effect on the overall performance of the CBR. In general, the flow resistance and thermal performance of the CBR raise synchronously with the decrease of the θ, β, and s, and the increase of d_w. Different flow patterns caused by the various geometric structures are the main reasons for the performance differences of the regenerators.
4. The multi-objective optimization was performed for minimizing the global friction factor f and maximizing the number of heat transfer units NTU by NSGA-II. The optimal combination of geometric parameters of $\theta = 10.91°$, $\beta = 29.25°$, $s = 1.512$ mm, and $d_w = 1.197$ mm was selected using the TOPSIS decision-making method. This optimal solution has been proven to present a superior performance within the range of studied geometric parameters by comparing with the extreme solutions.
5. In comparison with the commonly used traditional porous regenerators, the flow loss of the CBR is evidently decreased. Meanwhile, the CBR provides an excellent thermal performance slightly lower than the porous regenerators but significantly higher than the parallel geometry type regenerators. Moreover, the separation of the wire mesh layers indicates that an extremely low axial heat conduction loss will be generated in the CBR. Therefore, the CBR achieves a high comprehensive performance, which has the potential for improving the performance of Stirling engines.

Declaration of Competing Interest

The authors do not have any possible conflicts of interest.

CRediT authorship contribution statement

Minjie Yu: Conceptualization, Methodology, Software, Validation, Formal analysis, Investigation, Data curation, Writing – review & editing, Visualization. **Chunyu Shi:** Methodology, Software, Data curation, Writing – review & editing. **Zhichun Liu:** Conceptualization, Writing – review & editing, Resources, Supervision, Project administration, Funding acquisition. **Wei Liu:** Conceptualization, Writing – review & editing, Resources, Supervision.

Acknowledgments

This work was supported by the National Natural Science Foundation of China (Grant No. 51736004).

References

[1] I. Gunnarsdottir, B. Davidsdottir, E. Worrell, S. Sigurgeirsdottir, Sustainable energy development: history of the concept and emerging themes, Renew. Sustain. Energy Rev. 141 (2021) 110770.
[2] W.L. Chen, K.L. Wong, Y.F. Chang, A computational fluid dynamics study on the heat transfer characteristics of the working cycle of a low-temperature-differential γ-type Stirling engine, Int. J. Heat Mass Transf. 75 (2014) 145–155.
[3] D.D. Dai, F. Yuan, R. Long, Z.C. Liu, W. Liu, Imperfect regeneration analysis of Stirling engine caused by temperature differences in regenerator, Energy Convers. Manag. 158 (2018) 60–69.
[4] A.R. Tavakolpour, A. Zomorodian, A. Akbar Golneshan, Simulation, construction and testing of a two-cylinder solar Stirling engine powered by a flat-plate solar collector without regenerator, Renew. Energy 33 (1) (2008) 77–87.
[5] S.C. Costa, H. Barrutia, J.A. Esnaola, M. Tutar, Numerical study of the pressure drop phenomena in wound woven wire matrix of a Stirling regenerator, Energy Convers. Manag. 67 (2013) 57–65.
[6] S.C. Costa, H. Barrutia, J.A. Esnaola, M. Tutar, Numerical study of the heat transfer in wound woven wire matrix of a Stirling regenerator, Energy Convers. Manag. 79 (2014) 255–264.
[7] P. Bitsikas, E. Rogdakis, G. Dogkas, CFD study of heat transfer in Stirling engine regenerator, Therm. Sci. Eng. Prog. 17 (2020) 100492.
[8] W.L. Chen, K.L. Wong, Y.F. Chang, A numerical study on the effects of moving regenerator to the performance of a β -type Stirling engine, Int. J. Heat Mass Transf. 83 (2015) 499–508.
[9] Z. Buliński, A. Kabaj, T. Krysiński, I. Szczygieł, W. Stanek, B. Rutczyk, L. Czarnowska, P. Gładysz, A computational fluid dynamics analysis of the influence of the regenerator on the performance of the cold Stirling engine at different working conditions, Energy Convers. Manag. 195 (2019) 125–138.
[10] M. Arablu, A. Jafarian, Investigation of synchronous effects of multi-mesh regenerator and double-inlet on performance of a Stirling pulse tube cryocooler, Cryogenics 54 (2013) 1–9.
[11] S.K. Andersen, H. Carlsen, P.G. Thomsen, Numerical study on optimal Stirling engine regenerator matrix designs taking into account the effects of matrix temperature oscillations, Energy Convers. Manag. 47 (7-8) (2006) 894–908.
[12] B. Rutczyk, I. Szczygieł, A. Kabaj, Evaluation of an α type stirling engine regenerator using a new differential model, Energy 209 (2020) 118369.

[13] S. Isshiki, Y. Takasaki, I. Ushiyama, An experimental study on flow resistance of regenerator wire meshes in oscillatory flow, in: Proceedings of the 32nd Intersociety Energy Conversion Engineering Conference, IECEC-97, 1997, pp. 1027–1032.
[14] Y. Kato, K. Baba, Empirical estimation of regenerator efficiency for a low temperature differential Stirling engine, Renew. Energy 62 (2014) 285–292.
[15] M. Tanaka, I. Yamashita, F. Chisaka, Flow and heat transfer characteristics of the stirling engine regenerator in an oscillating flow, JSME Int. J. 33 (2) (1990) 283–289.
[16] D. Gedeon, J.G. Wood, in: Oscillating-Flow Regenerator Test Rig: Hardware and Theory with Derived Correlations for Screens and Felts, NASA CR-198442, 1996, pp. 6–13.
[17] W.L. Chen, K.L. Wong, H.E. Chen, An experimental study on the performance of the moving regenerator for a γ-type twin power piston Stirling engine, Energy Convers. Manag. 77 (2014) 118–128.
[18] R. Gheith, F. Aloui, S. Ben Nasrallah, Study of temperature distribution in a Stirling engine regenerator, Energy Convers. Manag. 88 (2014) 962–972.
[19] M. Ni, H. Peng, U. Sultan, K. Luo, G. Xiao, A quantitative method to describe the flow characteristics of an oscillating flow including porous media, Int. J. Heat Mass Transf. 119 (2018) 860–866.
[20] G. Xiao, H. Peng, H. Fan, U. Sultan, M. Ni, Characteristics of steady and oscillating flows through regenerator, Int. J. Heat Mass Transf. 108 (2017) 309–321.
[21] K. Nam, S. Jeong, Development of parallel wire regenerator for cryocoolers, Cryogenics 46 (4) (2006) 278–287.
[22] R. Tew, M. Ibrahim, D. Danila, T. Simon, S. Mantell, L. Sun, D. Gedeon, K. Kelly, J. McLean, J. Wood, S. Qiu, A microfabricated involute-foil regenerator for stirling engines, in: Proceedings of the International Energy Conversion Engineering Conference and Exhibit, St. Louis, Missouri, 2007, pp. 1–25.
[23] M.B. Ibrahim, D. Danila, T. Simon, S. Mantell, L.Y. Sun, A microfabricated segmented-involute-foil regenerator for enhancing reliability and performance of stirling engines: phase II final report for the radioisotope power conversion technology NRA contract NAS3-03124, Mech. Eng. Fac. Publ. (2007) 53–59.
[24] S. Isshiki, H. Sato, S. Konno, H. Shiraishi, N. Isshiki, L. Fujii, H. Mizui, The experimental study of atmospheric stirling engines using pin-fin arrays' heat exchangers, J. Power Energy Syst. 2 (2008) 1198–1208.
[25] Z. Li, Y. Haramura, Y. Kato, D. Tang, Analysis of a high performance model Stirling engine with compact porous-sheets heat exchangers, Energy 64 (2014) 31–43.
[26] Z. Li, Y. Haramura, D. Tang, C. Guo, Analysis on the heat transfer characteristics of a micro-channel type porous-sheets Stirling regenerator, Int. J. Therm. Sci. 94 (2015) 37–49.
[27] S. Alfarawi, R. Al-Dadah, S. Mahmoud, Potentiality of new miniature-channels Stirling regenerator, Energy Convers. Manag. 133 (2017) 264–274.
[28] S. Alfarawi, R. Al-Dadah, S. Mahmoud, Transient investigation of mini-channel regenerative heat exchangers: combined experimental and CFD approach, Appl. Therm. Eng. 125 (2017) 346–358.
[29] K. Yanaga, R. Li, S. Qiu, Robust foil regenerator flow loss and heat transfer tests under oscillating flow condition, Appl. Therm. Eng. 178 (2020) 115525.
[30] A. Bejan, Constructal-theory network of conducting paths for cooling a heat generating volume, Int. J. Heat Mass Transf. 40 (4) (1997) 799–816.
[31] A. Bejan, M.R. Errera, Convective trees of fluid channels for volumetric cooling, Int. J. Heat Mass Transf. 43 (17) (2000) 3105–3118.
[32] L. Chen, Q. Xiao, Z. Xie, F. Sun, Constructal entransy dissipation rate minimization for tree-shaped assembly of fins, Int. J. Heat Mass Transf. 67 (2013) 506–513.
[33] H. Feng, Z. Xie, L. Chen, Z. Wu, S. Xia, Constructal design for supercharged boiler superheater, Energy 191 (2020) 116484.
[34] H. Feng, C. Cai, L. Chen, Z. Wu, G. Lorenzini, Constructal design of a shell-and–tube condenser with ammonia-water working fluid, Int. Commun. Heat Mass Transf. 118 (2020) 104867.
[35] Z. Lu, K. Zhang, J. Liu, F. Li, Effect of branching level on the performance of constructal theory based Y-shaped liquid cooling heat sink, Appl. Therm. Eng. 168 (2020) 114824.
[36] M. Yu, F. Xin, X. Lai, H. Xiao, Z. Liu, W. Liu, Study of oscillating flows through a novel constructal bifurcation Stirling regenerator, Appl. Therm. Eng. 184 (2021) 116413.
[37] A. Abuelyamen, R. Ben-Mansour, Energy efficiency comparison of Stirling engine types (α, β, and γ) using detailed CFD modeling, Int. J. Therm. Sci. 132 (2018) 411–423.
[38] P.V. Trevizoli, J.R. Barbosa, Entropy generation minimization analysis of oscillating-flow regenerators, Int. J. Heat Mass Transf. 87 (2015) 347–358.
[39] R. Gheith, F. Aloui, S. Ben Nasrallah, Determination of adequate regenerator for a Gamma-type Stirling engine, Appl. Energy 139 (2015) 272–280.
[40] Q. Cao, L.M. Qiu, X.Q. Zhi, L. Han, Z.H. Gan, X.B. Zhang, X.J. Zhang, D.M. Sun, Impedance magnitude optimization of the regenerator in Stirling pulse tube cryocoolers working at liquid-helium temperatures, Cryogenics 58 (2013) 38–44.
[41] A.S. Nielsen, B.T. York, B.D. MacDonald, Stirling engine regenerators: how to attain over 95% regenerator effectiveness with sub-regenerators and thermal mass ratios, Appl. Energy 253 (2019) 113557.
[42] H. Solmaz, S.M. Safieddin Ardebili, F. Aksoy, A. Calam, E. Yılmaz, M. Arslan, Optimization of the operating conditions of a beta-type rhombic drive stirling engine by using response surface method, Energy 198 (2020) 117377.
[43] P. Yang, H. Chen, Y.W. Liu, Application of response surface methodology and desirability approach to investigate and optimize the jet pump in a thermoacoustic Stirling heat engine, Appl. Therm. Eng. 127 (2017) 1005–1014.
[44] W. Ye, X. Wang, Y. Liu, J. Chen, Analysis and prediction of the performance of free- piston Stirling engine using response surface methodology and artificial neural network, Appl. Therm. Eng. 188 (2021) 116557.
[45] F. Xin, Z. Liu, N. Zheng, P. Liu, W. Liu, Numerical study on flow characteristics and heat transfer enhancement of oscillatory flow in a spirally corrugated tube, Int. J. Heat Mass Transf. 127 (2018) 402–413.
[46] E. Dellali, S. Bégot, F. Lanzetta, E. Gavignet, J.Y. Rauch, Pressure drop analysis of oscillating flows through a miniature porous regenerator under isothermal and nonisothermal conditions, Exp. Therm Fluid Sci. 103 (2019) 394–405.
[47] H. Klein, G. Eigenberger, Approximate solutions for metallic regenerative heat exchangers, Int. J. Heat Mass Transf. 44 (2001) 3553–3563.
[48] M. Tutar, A. Holdø, Computational modelling of flow around a circular cylinder in sub-critical flow regime with various turbulence models, Int. J. Numer. Methods Fluids 35 (7) (2001) 763–784.